

## Twinned structure for shape memory: First-principles calculations

Xiao-Qian Wang

Department of Physics and Center for Functional Nanoscale Materials, Clark Atlanta University, Atlanta, Georgia 30314, USA

(Received 28 July 2008; published 8 September 2008)

We have performed first-principles calculations for the crystal structures of binary shape memory alloys NiTi, PdTi, and PtTi along with the transformation from austenite to martensite. A detailed analysis of the transition pathway shows that both the cubic  $B2$  and the orthorhombic  $B19$  evolve to a twinned structure followed by a transformation to the monoclinic  $B19'$ . In contrast to the low-energy body-centered orthorhombic structure for NiTi, the existence of this twinned state is essential for storing the shape memory in smart alloys.

DOI: 10.1103/PhysRevB.78.092103

PACS number(s): 61.66.Dk, 63.20.-e, 64.70.K-, 71.15.Mb

Shape memory alloys (SMAs) have attracted much attention in recent years as smart and functional materials due to the unique properties of shape memory smart functions and superelasticity.<sup>1-5</sup> Unlike the strained silicon micromechanical devices, NiTi-based SMAs do not suffer from extreme fragility and are ideal candidates for extreme critical applications in the automotive, aerospace, and electronics industries, and in mechanical engineering such as couplings, fasteners, connectors, and actuators.

From a metallurgical perspective, the principal properties of SMAs are explained by the solid-state phase transition called martensitic transformation (from the austenitic phase to the martensitic phase and vice versa). In spite of the technological importance of this type of materials, there is a striking lack of understanding of shape memory phenomena at the atomistic level. Several first-principles studies<sup>6-9</sup> have been performed for NiTi, PdTi, and PtTi. Despite the progress made, some questions remain regarding the relative stability of the martensite phases, as well as identifying the mechanisms that promote the shape memory behavior. This is, to a large extent, attributed to large number of parameters involved in martensitic structures. In this regard, Huang, Ackland, and Rabe (HAR) (Ref. 7) added a new wrinkle to this situation by identifying a body-centered orthorhombic (BCO) structure for NiTi. BCO is lower in energy than the experimentally observed monoclinic  $B19'$  phase, but it cannot store shape memory at the atomic level. Consequently, little progress has been made in construction of empirical interatomic potentials<sup>10</sup> and microstructure studies<sup>11</sup> due to the conflict between first-principles prediction and experimental results.

The phenomenological crystallographic theory for the shape memory effects involves three configurations: the austenite  $B2$ , a twinned martensite structure, and the monoclinic  $B19'$ . There are no previous calculations with respect to the twinned martensite structure although its existence is an important microstructural prerequisite for a crystalline solid to exhibit the shape memory effect. In addition, the twinned structure should be detwinable under stress. These conditions are satisfied in SMA systems in the loading and heating/cooling cycles.<sup>11,12</sup> In this Brief Report, we report on the results from first-principles calculations focusing on a twinned martensite structure capable of storing shape memory, which shed considerable light on the nature of the shape memory effect in smart alloys.

The first-principles calculations were performed using density-functional theory with a plane-wave pseudopotential approach, implemented through the Vienna *ab initio* simulation package (VASP).<sup>13</sup> The Perdew-Zunger parametrization of the local-density approximation (LDA) (Ref. 14) and Vanderbilt ultrasoft pseudopotentials<sup>15</sup> were used in most of the calculations, with a smearing parameter of 0.2 eV and a kinetic-energy cutoff of 242, 191, and 199 eV for NiTi, PdTi, and PtTi, respectively. For NiTi, calculations were also carried out using the Perdew-Burke-Ernzerhof<sup>16</sup> parametrization of the generalized gradient approximation (GGA). All calculations were performed using a  $9 \times 7 \times 7$  Monkhorst-Pack  $k$ -point mesh that corresponds to 128  $k$  points in the irreducible Brillouin zone. The  $k$ -point mesh ensures total-energy convergence to within 0.1 meV/atom for all structures.

We have performed calculations of various relevant SMA structures for NiTi, PdTi, and PtTi. In all cases, the high-temperature austenite phase has a simple cubic  $B2$  structure (space-group  $Pm\bar{3}m$ ), while the ambient temperature martensite phase has either an orthorhombic  $B19$  structure (space group  $Pmma$ ) or a monoclinic  $B19'$  structure (space group  $P2_1/m$ ). As seen in Fig. 1, the cubic  $B2$  involves a uniform expansion or contraction along the  $a$ ,  $b$ , and  $c$  directions, with equivalent  $ab$  and  $ac$  planes. The orthorhombic  $B19$  amounts to rearranging the atoms in the middle plane normal to  $c$  (in the direction of  $b$ ), resulting in a close-packed structure. Starting from  $B19$ , additional shear in the  $ab$  plane normal to  $c$  leads to a monoclinic  $B19'$  structure.

Shown in Table I are the calculated unit-cell parameters, atomic positions, and energy relative to  $B2$  of the  $B19$  and  $B19'$  structures for NiTi, PdTi, and PtTi. The calculated results agree with previous calculations, particularly in the energy order of martensite structures. The slight underestimate

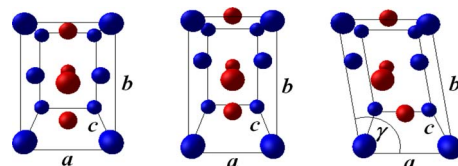


FIG. 1. (Color online) Unit cells for the cubic  $B2$  (left), the orthorhombic  $B19$  (middle), and the monoclinic  $B19'$  (right) crystal structures. Black (blue) and gray (red) balls represent Ni (Pd and Pt) and Ti atoms, respectively.

TABLE I. Calculated structural parameters (lattice constants  $a$ ,  $b$ , and  $c$ , monoclinic angle  $\gamma$ , and volume  $V$ ) in unit cells with  $P2_1/m$  space-group symmetry and energies relative to  $B2$  in  $B19$  and  $B19'$  compared to experimental (Ref. 12) and previous calculations [YCH (Ref. 6), HAR (Ref. 7), and HRA (Ref. 8)] results. The coordinates of the other two atoms can be determined by the symmetry of  $P2_1/m$ . The asterisk (\*) indicates the value was fixed in the calculation.

MTi	Structure	$a$ (Å)	$b$ (Å)	$c$ (Å)	$\gamma$ (°)	$V$ (Å <sup>3</sup> /atom)	$x_M$	$y_M$	$x_{Ti}$	$y_{Ti}$	$E-E_{B2}$ (eV/atom)
NiTi	$B19$	2.604	4.565	4.171	90	24.79	0	0.680	0.5	0.211	-0.046
	$B19$ (HAR)	2.657	4.567	4.178	90	25.34	0	0.681	0.5	0.214	-0.040
	$B19$ (YCH)	2.859	4.582	4.078	90	26.71	0	0.683	0.5	0.224	-0.034
	$B19'$	2.847	4.616	3.936	98.9	25.54	0.054	0.674	0.405	0.216	-0.051
	$B19'$ (HAR)	2.861	4.600	3.970	97.8*	25.88	0.044	0.674	0.413	0.217	-0.049
	$B19'$ (YCH)	2.892	4.598	4.049	97.8*	26.67	0.045	0.674	0.418	0.218	-0.046
	$B19'$ (Expt.)	2.898	4.646	4.108	97.8	27.40	0.037	0.675	0.418	0.216	
PdTi	$B19$	2.731	4.780	4.467	90	29.16	0	0.688	0.5	0.201	-0.074
	$B19$ (HRA)	2.745	4.812	4.486	90	29.63	0	0.687	0.5	0.201	-0.092
	$B19$ (YCH)	2.790	4.810	4.520	90	30.33	0	0.689	0.5	0.201	-0.092
	$B19'$	2.730	4.797	4.460	93.3	29.15	0.011	0.683	0.448	0.196	-0.076
	$B19'$ (HRA)	2.744	4.823	4.480	93.4	29.64	0.011	0.683	0.448	0.196	-0.092
PtTi	$B19$	2.730	4.769	4.524	90	29.46	0	0.689	0.5	0.198	-0.111
	$B19$ (HRA)	2.730	4.800	4.554	90	29.84	0	0.687	0.5	0.196	-0.151
	$B19$ (YCH)	2.810	4.830	4.550	90	30.88	0	0.688	0.5	0.197	-0.155
	$B19'$	2.731	4.794	4.506	93.5	29.45	0.015	0.684	0.446	0.192	-0.115
	$B19'$ (HRA)	2.736	4.821	4.531	93.6	29.88	0.015	0.684	0.446	0.191	-0.156

of the lattice constants and differences in energies can be attributed to the different pseudopotentials used. However, in contrast to the assessment of HAR,<sup>7</sup> we confirmed the existence of a locally stable  $B19'$  structure for NiTi that in fact can be obtained through geometry optimization starting from an experimentally observed configuration.<sup>12</sup> It is worth mentioning that the optimization with respect to the monoclinic angle is not continuous. The optimized monoclinic angle  $\gamma$  is 98.9°, slightly larger than the experimental value of 97.8°.<sup>12</sup>

Although the first-principles result for  $B2$ ,  $B19$ ,  $B19'$ , and BCO is readily available, it deals only with the initial (austenite) and final (martensite) states and it is not possible to argue the transformation path and time dependence of the martensitic transformation. To pursue the transition path, we have performed calculations using the nudged elastic band (NEB) method,<sup>17</sup> an efficient way to find the minimum-energy path. NEB defines the path as a sequence of images that are interpolated between the initial and final equilibrium structures, implemented such that the parallel component of the spring force defines path continuity while the perpendicular component of the force is minimized.

For NiTi, the NEB calculation for the transition pathway between the  $B19'$  and BCO structures shows that the two configurations are separated by an energy barrier of 0.01 eV/atom, thereby confirming that the  $B19'$  structure is locally stable. Interestingly, the evolution from  $B2$  or  $B19$  to  $B19'$  is through another distinct  $B19'$  structure with monoclinic angle  $\gamma \approx 96^\circ$ . At this point, it is instructive to consider structures with cell size doubled in the direction of  $b$  (with respect to results listed in Table I). With such a unit cell, twinned structures with  $Cmcm$  symmetry can be studied. The

optimization of the configuration constructed from twinning the distinct  $B19'$  structure yields a stable twinned state shown in Fig. 2.

Summarized in Table II are the structural parameters and the energy relative to  $B2$  for the twinned and BCO structures. To characterize the twinned structure, we can introduce a twinned angle,  $\gamma_T$ , defined in such a way that for the  $B19$  structure  $\gamma_T = 90^\circ$ , while for BCO  $\gamma_T$  coincides with the monoclinic angle  $\gamma$ . As can be seen from Fig. 2 and Table II, for NiTi the major differences between the twinned and BCO structures are the twinned angle, lattice constants ( $a$  and  $c$ ),

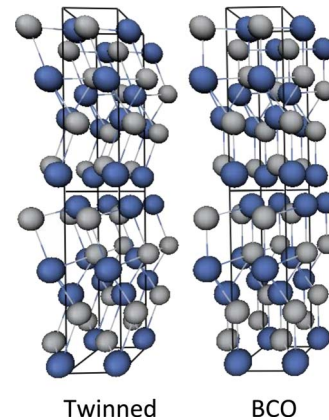


FIG. 2. (Color online) Perspective views of the twinned (left) and BCO (right) structures. Two orthogonal unit cells (doubled along the  $b$  direction) are shown. Black (blue) and gray balls represent Ni (Pd and Pt) and Ti atoms, respectively.

TABLE II. Calculated structural parameters (lattice constants  $a$ ,  $b$ , and  $c$ , twinned angle  $\gamma_T$ , and volume  $V$ ) in unit cells with  $Cmcm$  space-group symmetry and energies relative to  $B2$  in the twinned and BCO (for NiTi only) structures. The coordinates of the other six atoms can be determined by the symmetry of  $Cmcm$ .

MTi	Structure	$a$ (Å)	$b$ (Å)	$c$ (Å)	$\gamma_T$ (°)	$V$ (Å <sup>3</sup> /atom)	$x_M$	$y_M$	$x_{Ti}$	$y_{Ti}$	$E-E_{B2}$ (eV/atom)
NiTi	BCO	2.850	9.178	3.907	107.2	25.55	0	0.414	0	0.143	-0.053
	BCO (HAR)	2.864	9.242	3.933	107.2	26.02	0	0.415	0	0.143	-0.054
	Twinned	2.620	9.141	4.157	94.5	24.89	0.069	0.411	0.466	0.146	-0.049
	BCO (GGA)	2.947	9.454	4.038	107.3	28.13	0	0.415	0	0.144	-0.035
	Twinned (GGA)	2.772	9.406	4.266	97.4	27.81	0.071	0.412	0.407	0.143	-0.034
PdTi	Twinned	2.731	9.584	4.455	92.4	29.15	0.037	0.408	0.437	0.152	-0.077
PtTi	Twinned	2.731	9.558	4.493	93.1	29.32	0.048	0.408	0.428	0.155	-0.109

and the relative position of  $x_{Ti}$  and  $x_{Ni}$ . For NiTi, the GGA energy difference between the twinned structure and BCO is much smaller than the LDA energy difference,  $\sim 0.5$  meV/atom, and for PdTi, the twinned structure is lower in energy than  $B19'$ . The calculated (using GGA) elastic constants  $C_{11}$ ,  $C_{12}$ , and  $C_{44}$  are 162, 129, and 35 GPa, respectively, in excellent agreement with the experimental value of 165, 127, and 38 GPa for the martensite structure of NiTi.<sup>18</sup> It is worth noting that BCO is a special structure with  $B33$  symmetry not capable of storing the shape memory. In contrast, the twinning and parallel registry of  $B19'$  are distinct structures, and thus the cycle  $B2 \rightarrow$  twinned structure  $\rightarrow B19' \rightarrow B2$  can store shape memory.  $B2$  undergoes twinning as the temperature is lowered. The twinned structure can be deformed by external stress into a particular shape, and the crystal structure undergoes parallel registry. When heated, the deformed martensite  $B19'$  resumes its austenitic form.

Figure 3 shows the transition pathways calculated via the NEB method using unit cells consisting of eight atoms, with either four (from  $B2$  or  $B19$  to the twinned structure) or eight (from the twinned structure to  $B19'$  or BCO) interpolated images. In conformity with the phenomenological model, both  $B2$  and  $B19$  evolve to the twinned state, indicating that

the  $B2$  and  $B19$  structures are not stable against twinning at low temperatures. It is worth pointing out while BCO or  $B19'$  may be lower in energy than the twinned state, the twinning is largely independent of the energy order. For NiTi, the evolution from the twinned state to  $B19'$  goes through a transition state with a sudden change in orthorhombic lengths  $a$  and  $c$  relative to the twinned state, reminiscent of the loading induced transformations. For NiTi, the twinned state can also evolve to BCO. However, BCO is not stable under stress at the microstructure level.<sup>7</sup> In support of the conclusions made by HAR,<sup>7</sup> it is worth noting that the combination of a pair of  $B19$ ,  $B19'$ , and BCO configurations yields microstructure closely resembling a twinned structure. This point is particularly relevant in view of the recent experimental and theoretical studies emphasizing the importance of twinned structures.<sup>9,19</sup> On the other hand, the shape memory behavior for PdTi and PtTi is expected to experience much longer response time since the barrier between the twinned state and  $B19'$  is much higher (see inset of Fig. 3).

The martensite transformation temperature  $M_s$  is an important characteristic for high-temperature shape memory alloys. Ye, Chan, and Ho (YCH) (Ref. 6) suggested that there is a relationship between  $M_s$  and the difference in energy between the austenite and martensite phases. Noticing that  $B19$  can be considered as a shuffling to the  $B2$  structure along  $b$  with a coupling  $J_{\parallel} = E_{B19} - E_{B2}$ , while  $B19'$  or the twinned configuration undergoes additional shuffling with a coupling  $J_{\perp} = E_{B19'(TWIN)} - E_{B19}$ , it is expected that the symmetry-lowering shuffling distortions should disappear with an extremely anisotropic Ising-like transition. We may, quite roughly, use the formula of Ref. 20,  $k_B M_s \approx 2J_{\parallel} / \ln(J_{\parallel} / J_{\perp})$ , to get an estimate for  $M_s$ . It is gratifying that the estimated  $M_s$  is 440 (330 K using GGA), 480, and 780 K for NiTi, PdTi, and PtTi, respectively, in reasonable accordance with corresponding experimental values.<sup>6-8</sup>

In summary, we have demonstrated that the study of a twinned martensite structure is useful for understanding the mechanism of shape memory in smart alloys. The twinned structure for binary NiTi, PdTi, and PtTi identified in the present work can be viewed as the basic building block for constructing microstructural models of shape memory alloys. We remark, before closing, that it is straightforward to employ first-principles calculations to ternary shape memory

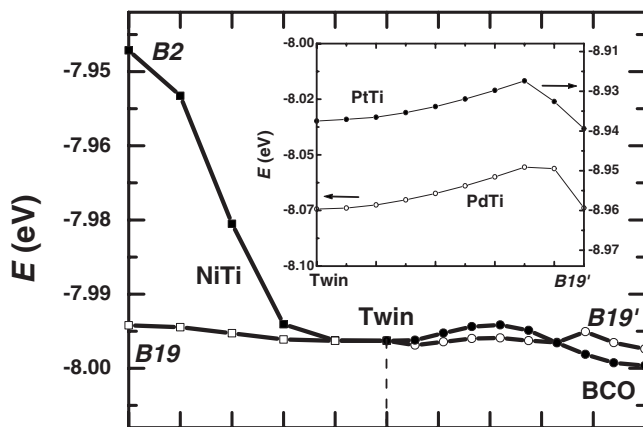


FIG. 3. The transition pathways of  $B2$  and  $B19$  evolving to  $B19'$  and BCO through the twinned structure and transition states for NiTi. The inset shows the transition pathways from the twinned structure to  $B19'$  for PdTi and PtTi.

alloys. For ternary alloys, the crystal structure can be reasonably constructed through stacking binary cells along the  $c$  direction, and the investigation of relevant martensite structures will provide an invaluable tool for developing high-temperature shape memory alloys complementing

experimental studies.<sup>5</sup>

The author thanks G. H. Bozzollo for fruitful discussions. This work was supported in part by the National Science Foundation (Grant No. DMR-02-05328) and Army Research Office (Grant No. W911NF-06-1-0442).

- 
- <sup>1</sup>K. Bhattacharya and R. D. James, *Science* **307**, 53 (2005).  
<sup>2</sup>W. W. Liang, M. Zhou, and F. J. Ke, *Nano Lett.* **5**, 2039 (2005).  
<sup>3</sup>H. S. Park, K. Gall, and J. A. Zimmerman, *Phys. Rev. Lett.* **95**, 255504 (2005).  
<sup>4</sup>M. Bouville and R. Ahluwalia, *Phys. Rev. Lett.* **97**, 055701 (2006); *Phys. Rev. B* **75**, 054110 (2007).  
<sup>5</sup>J. Cui, Y. S. Chu, O. O. Famodu, Y. Furuya, J. Hatrick-Simpers, R. D. James, A. Ludwig, S. Thienhaus, M. Wuttig, Z. Zhang, and I. Takeuchi, *Nat. Mater.* **5**, 286 (2006).  
<sup>6</sup>Y. Y. Ye, C. T. Chan, and K. M. Ho, *Phys. Rev. B* **56**, 3678 (1997).  
<sup>7</sup>X. Huang, G. J. Ackland, and K. M. Rabe, *Nat. Mater.* **2**, 307 (2003).  
<sup>8</sup>X. Huang, K. M. Rabe, and G. J. Ackland, *Phys. Rev. B* **67**, 024101 (2003).  
<sup>9</sup>T. Waitz, D. Spisak, J. Hafner, and H. P. Karnthaler, *Europhys. Lett.* **71**, 98 (2005).  
<sup>10</sup>M. S. Daw and M. I. Baskes, *Phys. Rev. B* **29**, 6443 (1984).  
<sup>11</sup>X. Wang and J. J. Vlassak, *Scr. Mater.* **54**, 925 (2006).  
<sup>12</sup>P. Villars and L. D. Calvert, *Pearson's Handbook of Crystallographic Data for Intermetallic Phases*, 2nd ed. (ASM International, Materials Park, OH, 1991).  
<sup>13</sup>G. Kresse and J. Furthmuller, *Phys. Rev. B* **54**, 11169 (1996); *Comput. Mater. Sci.* **6**, 15 (1996).  
<sup>14</sup>J. P. Perdew and A. Zunger, *Phys. Rev. B* **23**, 5048 (1981).  
<sup>15</sup>D. Vanderbilt, *Phys. Rev. B* **41**, 7892 (1990).  
<sup>16</sup>J. P. Perdew, K. Burke, and M. Ernzerhof, *Phys. Rev. Lett.* **77**, 3865 (1996).  
<sup>17</sup>G. Henkelman and H. Jónsson, *J. Chem. Phys.* **113**, 9978 (2000); G. Henkelman, B. P. Uberuaga, and H. Jónsson, *ibid.* **113**, 9901 (2000).  
<sup>18</sup>O. Mercier, K. N. Melton, G. Gremand, and J. J. Hagi, *J. Appl. Phys.* **51**, 1833 (1980).  
<sup>19</sup>M. E. Gruner, P. Entel, I. Opahle, and M. Richter, *J. Mater. Sci.* **43**, 3825 (2008).  
<sup>20</sup>C. Y. Weng, R. B. Griffiths, and M. E. Fisher, *Phys. Rev.* **162**, 475 (1967).